



Topoisomerase VI participates in an insulator-like function that prevents H3K9me2 spreading

Louis-Valentin Meteignier, Cécile Lecampion, Florent Velay, Cécile Vriet, Laura Dimnet, Martin Rougée, Christian Breuer, Ludivine Soubigou-Taconnat, Keiko Sugimoto, Fredy Barneche, et al.

► To cite this version:

Louis-Valentin Meteignier, Cécile Lecampion, Florent Velay, Cécile Vriet, Laura Dimnet, et al.. Topoisomerase VI participates in an insulator-like function that prevents H3K9me2 spreading. Proceedings of the National Academy of Sciences of the United States of America, 2022, 119 (27), 10.1073/pnas.2001290119 . hal-03862125

HAL Id: hal-03862125

<https://cnrs.hal.science/hal-03862125>

Submitted on 28 Nov 2022

HAL is a multi-disciplinary open access archive for the deposit and dissemination of scientific research documents, whether they are published or not. The documents may come from teaching and research institutions in France or abroad, or from public or private research centers.

L'archive ouverte pluridisciplinaire **HAL**, est destinée au dépôt et à la diffusion de documents scientifiques de niveau recherche, publiés ou non, émanant des établissements d'enseignement et de recherche français ou étrangers, des laboratoires publics ou privés.



Distributed under a Creative Commons Attribution - NonCommercial - NoDerivatives 4.0 International License

Topoisomerase VI participates in an insulator-like function that prevents H3K9me2 spreading.

Louis-Valentin Méteignier¹, Cécile Lecampion¹, Florent Velay¹, Cécile Vriet^{1,2}, Laura Dimnet¹, Michel Tère³, Martin Rougée^{4,5}, Christian Breuer⁶, Ludivine Soubigou-Taconnat^{7,8}, Keiko Sugimoto⁶, Fredy Barneche^{4,5} and Christophe Laloi^{1*}.

¹Aix Marseille Univ, CEA, CNRS, BIAM, Marseille, France F-13009

²UMR CNRS 7267, University of Poitiers, 86073 Poitiers Cedex

³Independent informatician, 06100 Nice, France

⁴IBENS, Département de Biologie, Ecole Normale Supérieure, CNRS, PSL Research University, F-75005, Paris, France

⁵Université Paris-Sud, Université Paris-Saclay, 91405, Orsay, France.

⁶RIKEN Center for Sustainable Resource Science, Yokohama, 230-0045, Japan

⁷Institute of Plant Sciences Paris Saclay IPS2, CNRS, INRA, Université Paris-Sud, Université Evry, Université Paris-Saclay, Bâtiment 630, 91405 Orsay, France.

⁸Institute of Plant Sciences Paris-Saclay IPS2, Paris Diderot, Sorbonne Paris-Cité, Bâtiment 630, 91405, Orsay, France

Corresponding author:

Christophe Laloi, christophe.laloi@univ-amu.fr

Classification:

BIOLOGICAL SCIENCES: Plant Biology

Keywords

Euchromatin islands / Heterochromatin spreading / Insulator / Methionine Adenosyltransferase / Topoisomerase VI.

Abstract

The organization of the genome into transcriptionally active and inactive chromatin domains requires well-delineated chromatin boundaries and insulator functions in order to maintain the identity of adjacent genomic loci with antagonistic chromatin marks and functionality. In plants that lack known chromatin insulators, the mechanisms that prevent heterochromatin spreading into euchromatin remain to be identified. Here, we show that DNA Topoisomerase VI participates in a chromatin boundary function that safeguards the expression of genes in euchromatin islands within silenced heterochromatin regions. While some transposable elements are reactivated in mutants of the Topoisomerase VI complex, genes insulated in euchromatin islands within heterochromatic regions of the *Arabidopsis thaliana* genome are specifically downregulated. H3K9me2 levels consistently increase at euchromatin island loci and decrease at some TE loci. We further show that Topoisomerase VI physically interacts with S-adenosylmethionine (SAM) synthase MAT3, which is required for H3K9me2. A Topoisomerase VI defect affects MAT3 occupancy on heterochromatic elements and its exclusion from euchromatic islands, thereby providing a possible mechanistic explanation to the essential role of Topoisomerase VI in the delimitation of chromatin domains.

Significance Statement

In the eukaryotic genome, DNA associates with proteins and form two main types of chromatin, the highly condensed heterochromatin, which is inaccessible to transcription factors and hence transcriptionally silent, and the less condensed, hence transcriptionally active euchromatin. The maintenance of sharp boundaries between these chromatin domains with antagonistic functionality is therefore critical for transcriptional control and involves chromatin insulators that remain unknown in plants. Here, we show that a plant topoisomerase participates in such a chromatin boundary function that prevent heterochromatin spreading into euchromatin and hence safeguards the expression of genes in euchromatin islands within silenced heterochromatin regions. We have also identified partners of this topoisomerase that allow us to provide a mechanistic insight to this insulator-like function.

Introduction

The discovery of position effect variegation in *Drosophila melanogaster* paved the way towards revealing the importance of chromatin contexts in the regulation of gene expression (1, 2). Since then, cytogenetic and molecular profiling of the epigenome, as well as topological analyses of chromatin architecture, have allowed the mechanisms involved in partitioning the gene-rich euchromatic fraction from the repeat-rich heterochromatic fraction to be elucidated. Large protein complexes specific to insulator DNA sequences contribute to partitioning chromatin domains with distinct identity at multiple scales. These complexes maintain the identity of adjacent genomic loci with antagonistic chromatin marks and functionality, and more globally influence the formation of long-range chromosomal interactions (3). Insulator binding proteins such as the CCCTC-binding factor CTCF, BEAF-32, CP190 and Mod have been best described in *Drosophila* where they play critical roles in the definition of chromatin and transcriptional status. In vertebrates, CTCF is the only known insulator binding protein homologue. CTCF is enriched at insulator DNA sequences that define large topological domains of the genome (4–6) and, in some cases, define boundaries between adjacent chromatin domains with distinct features (7). Surprisingly, CTCF orthologs cannot be identified in many eukaryotic organisms, including plants (8). Moreover, very few studies support the presence of insulator DNA sequences or insulator-like regions in plants (9–11), and insulator binding factors remain to be identified. This contrasts with the observation that *Arabidopsis thaliana* and other plant species display highly indexed chromatin states along the genome, with well-defined chromatin signatures around transcriptionally active or repressed genes, as well as close relationships between chromatin composition and genome topology in the nuclear space (12, 13). In *Arabidopsis*, heterochromatin is found on hundreds of transposable elements (TEs) mostly confined within the pericentromeric regions and at a few knob structures that tend to associate through long-distance interactions in the nuclear space (14–18). As a result, in *Arabidopsis* interphase nuclei most cytologically visible heterochromatin is condensed within 8 to 10 conspicuous foci that are referred to as chromocenters (19–21). Consistent with their heterochromatic nature, chromocenters are refractory to transcription and contain highly methylated DNA (22) as well as histone modifications such as H3K9me2 and H3K27me2 (23, 24). Nonetheless, many expressed genes exhibiting euchromatic features appear to be located in close vicinity to large heterochromatic regions in the *Arabidopsis* genome, notably within the pericentromeric and knob regions (25, 26). The mechanisms by which gene-containing euchromatic islands (EIs) are insulated from neighboring heterochromatin regions and how their transcriptional capacities are preserved in such chromatin contexts are largely unknown. In this study, we have unveiled an essential function of the plant Topoisomerase VI complex in preserving the functional and structural identity of EIs.

DNA topoisomerases are enzymes that introduce transient DNA breaks to resolve topological constraints that arise during multiple cellular processes such as replication, transcription, recombination and chromatin remodeling. The plant Topo VI, a type II topoisomerase first identified in the archaeon *Sulfolobus shibatae* (27, 28), was initially implicated in various biological processes involving endoreduplication, such as root hair growth (29–31), hypocotyl elongation (31) and nodule differentiation (32). Topo VI forms an A₂B₂ heterotetramer whose A and B subunits are encoded by single genes in *Arabidopsis*, *AtTOP6A/CAA39/AtSPO11-3/RHL2/BIN5/AT5G02820* and *AtTOP6B/RHL3/BIN3/HYP6/HLQ/AT3G20780*, respectively (33–37). Two additional subunits named ROOT HAIRLESS 1 (RHL1/HYP7/AT1G48380) and BRASSINOSTEROID-INSENSITIVE 4 (BIN4/MID/AT5G24630) (31, 38, 39) are essential for the *Arabidopsis* Topo VI function and appear to be evolutionarily conserved in plants and in other eukaryote groups, whilst their precise functions remain unclear. However, BIN4 shares sequence similarity with the C-terminal region of animal Topo II α , which seems to have regulatory functions (40–42), and exhibits stable DNA binding *in vitro* (38). Therefore, it has been proposed that BIN4 may have a regulatory role in the plant Topo VI complex, presumably by holding the substrate DNA through its AT-hook motif (38, 39).

In recent years, evidence has accumulated that topoisomerases have more diverse and specialized functions than previously thought (43). In particular, transcriptomic analyses of several Topo VI mutants revealed that Topo VI influences the expression of many nuclear genes, including genes regulated by phytohormones (35, 36) or by reactive oxygen species (44–46). A function of *Arabidopsis* Topo VI as a chromatin-remodeling complex has also been speculated (35). This hypothesis has since been supported by the observation that loss of the Topo VI B subunit in *hlq* mutant plants leads to the mis-expression of numerous adjacent genes, hence possibly triggering positional or chromatin context dependent transcriptional defects (36). This is further supported by the implication of the BIN4 subunit in heterochromatin organization, as observed by smaller and diffuse chromocenters in interphase nuclei of plants bearing the severe *mid* mutation (39).

Here, we reveal that *Arabidopsis* Topo VI is required for chromocenter formation and for efficient silencing of some heterochromatic TEs but has an antagonistic effect on genes localized in euchromatic islands (EIs). Downregulation of EI genes in Topo VI mutant plants is associated with an enrichment of the H3K9me2 heterochromatic mark. We further report that the BIN4 subunit of Topo VI directly interacts with S-adenosylmethionine (SAM) synthetase 3 / Methionine Adenosyl transferase 3 (MAT3). Similar to Topo VI knockdown plants, *mat3* knockdown mutants exhibit de-repression of heterochromatic TEs and a decrease in H3K9me2. Furthermore, we show that the association of MAT with heterochromatic elements is reduced in a hypomorphic Topo VI mutant, whereas it increased at some EIs. We therefore propose that Topo VI has a prominent role in the

delimitation of chromatin boundaries, could participate in defining SAM synthesis sites onto specific regions of the genome, and collectively has an essential role in the establishment of distinct chromatin domains.

Results

Topoisomerase VI is required for heterochromatin organization

Kirik *et al.* reported that interphase nuclei of the severe *mid* mutant in the BIN4/MID subunit presents smaller and less defined chromocenters (CCs) compared to the wild-type (wt), suggesting that heterochromatin organization is affected by the *mid* mutation (39). However, this phenotype was not reported in the allelic *bin4-1* mutant, which also has a severe phenotype (38). Therefore, to unequivocally confirm the role of the *Arabidopsis* Topo VI complex in nuclear organization, we analyzed the nuclear phenotypes of hypomorphic and amorphic mutants of the AtTOP6A subunit, *caa39* and *rhl2-1*, and of the BIN4/MID subunit, a *BIN4* knockdown line (*BIN4* KD, see below) and *bin4-1*, by DAPI DNA staining and immunolocalization of heterochromatin hallmarks. Both the *caa39* and *rhl2-1* mutants exhibited strong alterations in heterochromatin organization with largely decondensed chromocenters (Fig 1A, top panel, and SI Appendix, Fig S1A). Likewise, nuclei of epidermal and mesophyll cotyledon cells from *BIN4* KD and *bin4-1* did not harbor conspicuous chromocenters (SI Appendix, Fig S1A), as previously reported for the *mid* allelic mutants (39). In contrast, the nuclear phenotype of shoot apical meristematic cells is similar in wt, *caa39*, *rhl2-1*, *bin4-1* and *BIN4* KD lines, with equal proportions of nuclei with conspicuous (type 1) or diffuse (type 2) chromocenter profiles (SI Appendix, Fig S1A, meristem panel, and Fig S1B). Consistent with its role in endocycles but not in mitosis (31, 37–39), these defects indicate that Topo VI is required for chromatin organization of differentiated cells, but less of actively dividing cells. Immunofluorescence analysis of the heterochromatin hallmark H3K9me2 confirmed the large extent of heterochromatin decondensation in *caa39* Topo VI mutant plants (Fig 1A). Immunoblot analyses further showed that the global level of H3K9me2 is not affected in *caa39* seedlings (Fig 1B). Likewise, 5-methylcytosine (5-meC) immunolabeling also revealed a dispersed signal in *caa39* nuclei (Fig 1C) whereas an anti-5-meC ELISA showed overall similar levels of 5-meC in wt and *caa39* as compared to *ddm1-8* seedlings (Fig 1D). These results suggest that the marked alteration of chromocenter morphology does not result from a global decrease in heterochromatin hallmarks in *caa39*.

Topo VI is required for the silencing of heterochromatic transposable elements

A role for *Arabidopsis* Topo VI in heterochromatin-dependent transcriptional gene silencing was highlighted by the reactivation of *TRANSCRIPTIONALLY SILENT INFORMATION (TSI)* in *mid* mutant plants (39). However, reactivation was not observed in the *bin4-1* allelic mutant (38). Therefore, to unambiguously assess the involvement of Topo VI in transcriptional silencing and get a more global understanding of Topo VI influence on TE repression, we performed a RNA-seq analysis of *caa39* and wt transcripts. Multiple heterochromatic TEs (176 TEs with $\log_2(\text{FC}) > 2$), particularly from the LTR/Gypsy, LTR/Copia and En-Spm/CACTA superfamilies (47), are reactivated in *caa39* plants (Fig 2A, Dataset S1). Conversely, 91 TEs are repressed in *caa39* ($\log_2(\text{FC}) < -2$); unlike reactivated TEs, these repressed TEs are rarely in the most inaccessible and repressive heterochromatin state 9 (SI Appendix, Fig S2A). To test for TE silencing defects in other Topo VI mutants, we selected several de-repressed heterochromatic TEs loci (Dataset S1) for which robust primer design was feasible, and measured their relative transcript abundance by RT-qPCR in *rh12-1* and *bin4-1* mutants along with the *caa39* and wt lines. A clear increase in TE transcript abundance was observed for all three tested Topo VI mutant lines (Fig 2B).

Although we found no global decrease of H3K9me2 and 5-meC in *caa39* (Fig 1B and 1D), more subtle local changes could account for TE reactivation. We first assessed DNA methylation levels at individual TEs in Topo VI mutants as compared to wt and *ddm1-8* plants by digestion with the methylation-dependent restriction enzyme McrBC. As expected, very efficient digestion of TEs was observed in wt but not in *ddm1-8* plants, reflecting a nearly complete loss of DNA methylation over multiple TEs in this hypomethylated mutant line (Fig 2C). In sharp contrast, we observed wt levels of DNA methylation for all tested loci in *caa39* and *bin4-1* plants. This trend was confirmed in different sequence contexts (CG, CHG and CHH) by using the methylation-sensitive restriction enzymes HpaII, MspI and HaeIII (SI Appendix, Fig S3). Similar DNA methylation levels of TEs in wt and *caa39* were then confirmed genome-wide by whole-genome bisulfite sequencing, in all three contexts (Fig 2D). We concluded that TE de-repression in Topo VI mutants could not be accounted for by a global decrease of DNA methylation in *cis*. Next, we measured the level of H3K9me2 at TEs, which could be performed only with the *caa39* hypomorphic mutant, owing to the extreme dwarf phenotype of the *rh12-1* and *bin4-1* null mutants. ChIP-qPCR analyses revealed a modest decrease in H3K9me2 at some but not all tested TEs in *caa39* as compared to wt plants (Fig 2E). ChIP-seq analysis of H3K9me2 levels in wt and *caa39*, normalized to H3 levels in each line, confirmed the slight decrease of H3K9me2 at *AT3TE60425* and *AT4TE15030*, but not at *AT2TE15415* and *AT4TE16900* (SI Appendix, Fig S2B-C), and revealed a significant global decrease ($P < 0.01$, Mann-Whitney test) of H3K9me2 at TEs (Fig 2F). Collectively, these results suggest that H3K9me2 local decreases and

heterochromatin spatial reorganization may contribute to TE activation, although the precise causal mechanism is unknown.

Unlike TEs, genes interspersed within pericentromeric and chromosome 4 knob large heterochromatin regions are massively downregulated in Topo VI mutants

We then used the online positional gene enrichment tool (48) to investigate the genomic distribution of misregulated genes identified in our RNA-seq analysis of *caa39* (Dataset S2). This analysis revealed that the 500 most downregulated genes are strikingly over-represented in pericentromeric regions (PRs) and in the heterochromatic knob of chromosome 4 (*hk4S*, Fig 3A). In these regions, 94% (181/193) of the non-TE genes that are differentially expressed in *caa39* are downregulated (Dataset S2). In contrast, the 500 most highly upregulated genes displayed no preferential localization (SI Appendix, Fig S4A). To determine whether this effect is robust in other Topo VI mutant lines, we first examined the expression profiles of *bin4-1* and a second allelic mutant, *bin4-2*, from microarray data that were generated during the initial characterization of these two allelic lines (38). Despite the fact that *bin4-1* and *bin4-2* are knock-out mutants that have much more severe developmental defects than *caa39*, and although two different technical platforms have been used (RNA-seq for *caa39* vs Affymetrix ATH1 microarrays for *bin4-1* and *bin4-2*), we found a good correlation between the different transcriptomes (SI Appendix, Fig S4B). In particular, 91% (72/79) of the PR genes that are repressed in *caa39* and are detected in both RNA-seq and microarray experiments are also downregulated in *bin4-1* or *bin4-2* (Fig 3B, Dataset S2). We examined further the expression of seven pericentromeric genes distributed over the five chromosomes and strongly repressed in *caa39*, by RT-qPCR in *caa39*, *bin4-1* as well as in *rh12-1* plants. These genes were found to be downregulated in all mutants, except for *AT4G06634* and *AT4G07390* that were not significantly repressed in *rh12-1* and *bin4-1* (Fig 3C). This could possibly be due to secondary effects of the *bin4-1* and *rh12-1* amorphic mutations as compared to the less severe *caa39* mutation. In order to test this hypothesis, we took advantage of the availability of an *Arabidopsis* *BIN4* co-suppressed transgenic line identified during the process of generating lines overexpressing *BIN4-CFP*. Rather than exhibiting *BIN4* upregulation, this *BIN4* KD homozygous, mono-insertional transgenic line, shows downregulation of *BIN4* (SI Appendix, Fig S5A-B) and develops a phenotype similar to *caa39* (SI Appendix, Fig S5C). In this line, all tested pericentromeric genes were at least as much downregulated as in *caa39*, with a more pronounced effect than in the *bin4-1* and *rh12-1* knockout mutants (Fig 3C). These observations indicate that Topoisomerase VI is required to maintain

transcriptional control of both genes and TEs in pericentromeric and *hk4S* regions, possibly acting as a chromatin architectural factor.

Downregulated genes within heterochromatic regions are localized in small euchromatic islands

We then asked whether the inverse expression patterns of genes and TEs in pericentromeric and *hk4S* regions in Topo VI mutants could be ascribed to their different chromatin landscapes. We first inspected the individual chromatin landscape of the seven downregulated pericentromeric genes confirmed by RT-qPCR (Fig 3C), using the nine chromatin states defined by Sequeira-Mendes *et al.* (49). Euchromatin states 2, 1 and 3 characterize the proximal promoter, the transcriptional start site, and the start of coding sequence, respectively. The intragenic states 6 and 7 are characteristic of the transcriptional termination site and gene body of long transcribed genes, respectively. States 4 and 5 are highly enriched in H3K27me3 (a *Polycomb*-Repressive Complex 2 (PRC2)-based repressive histone modification) and are usually found in intergenic regions and PRC2-targeted genes. Lastly, the two types of heterochromatin states, 8 and 9, are enriched in H3K9me2, but in contrast with state 8, state 9 preferentially defines pericentromeric heterochromatin and is devoid of H3K27me3 (49). Strikingly, all inspected loci share common features: a typical euchromatin context whose proximal environment is composed of heterochromatic state 8 and whose distal environment is of heterochromatic state 9 (SI Appendix, Fig S6A). Overall, these observations suggested that *caa39* downregulated genes might be part of *bona fide* euchromatic islands (EIs).

To generate a comprehensive view of their structural features in the genome, we systematically investigated the pericentromeric and *hk4S* heterochromatic regions defined in Appendix Figure S6B. We designed a script to extract all EIs surrounded by chromatin states 8 and 9, then we analyzed the proportion of chromatin states covering EIs and their 1.5 kb flanking regions (Fig 3D). We identified 232 EIs containing 540 EI genes this way, among which 6 correspond to unsequenced gaps (<https://jbrowse.arabidopsis.org/?data=Araport11>) and were discarded in subsequent analyses (Dataset S3). Looking for EIs directly flanked by state 9 chromatin did not increase the number of EIs identified, showing that chromatin state 8 is always present in the proximal border (Fig 3D, SI Appendix, Fig S6C). In contrast, the number of detected EIs started to decrease to 215 when considering two-nucleosome-long flanking regions in state 8, suggesting that 11 EIs have only one proximal nucleosome in state 8 (SI Appendix, Fig S6C). With respect to state 9, the number of extracted islands began to drop from 4-nucleosome-long flanking regions, suggesting that the state 8 proximal border is always flanked by at least 3-nucleosome-long state 9 regions (SI

Appendix, Fig S6C). A majority of EIs (157/232) are short and contain only one or two genes (Fig. 3E, Dataset S3, SI Appendix, Table S1).

Topo VI prevents the spreading of H3K9me2 into euchromatic islands

Given the general repression of EI genes and the local decrease of H3K9me2 at some TE loci without affecting the global level of H3K9me2 (Fig 1B), we hypothesized that EI gene repression might result from ectopic spreading of this silencing mark over EIs. This was first tested on several EI genes by ChIP-PCR analysis of H3K9me2 levels in wt and *caa39*. H3K9me2 levels were very low, barely above background, in wt, consistent with the fairly high level of expression of these genes (Fig 4A). In contrast, a clear increase of H3K9me2 was observed in *caa39* (Fig 4A). Therefore, we further tested the spreading of H3K9me2 over EIs on a genome-wide scale by ChIP-seq analysis of H3K9me2 levels in wt and *caa39*, normalized to H3 levels in each line. Analysis of the wt profile showed short EIs (S-EIs, which contain only one or two genes and are < 6kb-long) with sharp boundaries and where H3K9me2 was barely detected, flanked by regions with high H3K9me2 levels (Fig 4B). Consistent with the minor decrease observed only on some TEs presented in Figure 2, the H3K9me2 level is globally not lower in EI-flanking sequences in *caa39* as compared to wt. In contrast, a clear increase was observed within S-EIs of *caa39*, which was highly significant all along S-EIs (Mann-Whitney test, Benjamini-corrected $P < 0.01$), suggesting that Topo VI prevents H3K9me2 spreading across natural boundaries (Fig 4B). H3K9me2 spreading into large and more complex EIs (L-EIs, > 6kb-long and often containing internal state 8) was also highly significant and particularly pronounced on L-EIs boundaries (Fig. 4C). Inspection of meta-profiles for each chromosome confirmed highly significant H3K9me2 spreading into EIs (SI Appendix, Fig S7A), that was observed for all replicates (SI Appendix, Fig S7B).

To further strengthen our analysis, we applied diffReps (50) on each replicate individually to confirm differential enrichment of H3K9me2 in EIs of *caa39* and wt (Dataset S4). This very stringent and not very sensitive analysis (essentially due to the fact that H3K9me2 peaks were barely detectable in wt and that H3K9me2 spreading does not appear to be sequence-specific) could still reveal increased levels of H3K9me2 in some EIs of *caa39*, but not all (92.0% in replicate 2, 73.9% in replicate 3, 27.4% in replicate 1; Dataset S3). The limited number of EIs identified this way in replicate 1 can be attributed to the fact that it was less deeply sequenced than replicates 2 and 3 (GSE103924). Despite that, there was a large overlap between replicates: among EIs that showed increased levels of H3K9me2 in *caa39*, only one was identified in replicate 1 but not in replicates 2 or 3, and 96.4% (161/167) of the EIs identified in replicate 3 were also identified in replicate 2 (SI

Appendix, Fig S7C, Dataset S3). We then extracted the number of significantly (diffReps G-test, $P < 0.01$) up or down H3K9me2 peaks in *caa39* versus wt, in each individual replicate (Dataset S4, sheet 4). A similar percentage of significantly up or down H3K9me2 peaks was observed at the genome scale by this method (Fig 4D), in agreement with the fact that the global level of H3K9me2 does not seem to be significantly affected in *caa39*. In contrast, the proportion of peaks was significantly shifted toward gains of H3K9me2 within EIs, particularly within EI genes and their 5' UTRs (Fig 4D, Dataset S4), confirming the specific role of Topo VI in safeguarding EI genes from ectopic spreading of H3K9me2.

Globally, these data show that Topo VI is required to prevent elevated H3K9me2 levels within EIs, presumably by preserving sharp boundaries between these insulated elements to avoid pervasive spreading of heterochromatin from flanking regions. We further documented such a barrier-like function on a S-EI containing a single gene, *At1g41830*, by ChIP-qPCR analysis of H3K9me2. Scanning of six different loci along this region (Fig 4E) in independent experiments confirmed the increased H3K9me2 levels within the island body, but also a decrease in one neighboring heterochromatic border (Fig 4E), similarly to what was observed in the ChIP-seq experiment replicates for this EIs (Fig 4I and SI Appendix, Fig S8) and other inspected EIs (SI Appendix, Fig S8).

EI gene repression is correlated with H3K9me2 spreading

We then tried to evaluate the relative contribution of H3K9me2 increase to the downregulation of EI genes, compared to other heterochromatin and repressive marks. Firstly, because H3K9me2 and non-CG (CHG and CHH) DNA methylation are strongly inter-dependent (51), we tested whether H3K9me2 spreading into EIs might in turn, or reciprocally, affect DNA methylation. Whole-genome bisulfite sequencing revealed that DNA methylation levels in all sequence contexts were overall unaltered in *caa39* relative to wt in EIs (Fig 4F and I, SI Appendix, Fig S8). Differentially methylated region (DMR) analyses confirmed that there was no global significant increase of DNA methylation in EIs (Dataset S5). Surprisingly, despite CHGs being known to be methylated through a feedback loop with H3K9me2, DMR analyses rather revealed a very slight decrease of CHG, with 51 hypo-CHG DMRs and 16 hyper-CHG DMRs observed in EIs of *caa39* (with differences in the methylation percentage higher than 10%, $P < 0.05$, Dataset S5). Therefore, DNA methylation does not seem to contribute to the downregulation of gene expression in EIs.

Secondly, because EI boundaries are enriched in H3K27me3-marked heterochromatin state 8, and that H3K27me3 is also found on the proximal promoter (chromatin state 2) and transcribed

region of many euchromatic genes (chromatin state 5, silenced genes) (49), we also performed a genome-wide H3K27me3 analysis by ChIP-seq. Interestingly, we observed a globally inverted tendency as compared to H3K9me2 profiles: average H3K27me3 levels were locally and significantly decreased within EIs (SI Appendix, Fig S9A-B). We further documented such a local decrease of H3K27me3 on the S-EI containing *At1g41830*, by ChIP-qPCR (SI Appendix, Fig S9C). Consistent with this, K-means linear clustering revealed that H3K27me3 decrease could not be generalized to all EIs, as it marks only a small subset of EIs in wt (Fig 4G). Thus, H3K27me3 does not seem to contribute to the global downregulation of EI genes, and its local decrease at some EI genes might even counterbalance the effect of H3K9me2 increase in a few EIs.

Finally, we directly compared EI gene expression with H3K9me2 changes. A vast majority (90%) of EI genes that show significant changes ($P < 0.05$) in either RNA-seq or ChIP-seq analyses are repressed and possess enhanced levels of H3K9me2 (Fig 4H and I, SI Appendix, Fig S8 and S10A). Interestingly, the most repressed genes also tend to have the sharpest H3K9me2 increase, which is particularly true in S-EIs. (Fig 4H, SI Appendix, Fig S10A). To see whether H3K9me2 defect might affect the expression of EI genes, we generated the quadruple mutant *caa39 suvh456* mutated for the H3K9 methylase genes *KRYPTONITE (KYP)/ SUVH4*, *SUVH5* and *SUVH6* and examined the expression of the seven pericentromeric genes already studied. The expression of some EI genes was significantly increased in *caa39 suvh456* as compared to *caa39* (Fig S10B). Taken together, these results suggest that H3K9me2 increase plays a role in the reduced expression of EI genes, although higher order chromatin structure, changes in other histone modification, and other indirect effects of the *caa39* mutation may contribute to gene expression changes.

The Topo VI subunit BIN4 physically associates with MAT3

To gain knowledge on the molecular mechanism by which Topo VI contributes to the delimitation of chromatin boundaries, we used the BIN4 subunit as a bait to screen a yeast two hybrid (Y2H) cDNA library (Hybrigenics). A strong interaction with the Topo VI subunit RHL1 was detected, thereby demonstrating the reliability of the screening procedure (Dataset S6). Among the eleven additional interacting partners, three proteins belong to the S-AdenosylMethionine (SAM) biosynthesis pathway, the universal methyl group donor (52). The first one, 5-methylthioribose-1-phosphate isomerase (MTI1, AT2G05830), is involved in the methionine salvage pathway whereas the two others, Methionine Synthase 1 (MS1, AT5G17920) and Methionine Adenosyltransferase 3 (MAT3, AT2G36880) are the ultimate enzymes of the SAM cycle. In order to identify BIN4-interacting proteins *in planta*, we also performed a CoIP-MS experiment using the *Arabidopsis mid-1*

354 35S:*BIN4/MID-YFP* line, which consists of the *mid-1* allelic mutant of *BIN4* complemented with YFP-
355 tagged *BIN4/MID* (39), and a wt line as control. To exclude nonspecific proteins, we discarded
356 proteins that were not detected in both *BIN4/MID-YFP* CoIP-MS replicates, as well as plastidial,
357 mitochondrial and peroxisomal proteins. The presence of the RHL1 and TOP6B Topo VI subunits in
358 *BIN4/MID-YFP* CoIPs validated our procedure (Dataset S7). Remarkably, *MAT3* co-
359 immunoprecipitated strongly with *BIN4*. *MAT4* also co-immunoprecipitated with *BIN4*, but
360 apparently to a much lesser extent (Dataset S7). We further investigated the genetic and biochemical
361 interactions between *BIN4* and enzymes of the SAM cycle, particularly the very last enzyme *MAT3*,
362 using Bimolecular Fluorescence Complementation (BiFC). We confirmed the *BIN4-MAT3* and *BIN4-*
363 *MS1* interactions in nuclei of transiently agro-transformed *Nicotiana benthamiana* mesophyll cells
364 (Fig 5A).

366 **MAT3 is required for H3K9me2**

367 Given that MAT enzymes synthesize the SAM required for DNA and histone methylation, and
368 that Topo VI is required for proper distribution of H3K9me2 throughout EI-containing
369 heterochromatic regions, we hypothesized that disruption of *MAT3* affects H3K9me2 deposition. To
370 address this question, we used a recently characterized knock-down line in which *MAT3* 3'-UTR is
371 interrupted by a T-DNA (53), generating strongly reduced but still detectable transcripts levels (SI
372 Appendix, Fig S11A). We measured H3K9me2 levels at the four TEs strongly de-repressed in Topo VI
373 mutant plants (Fig 2) by ChIP-qPCR and found decreased levels of H3K9me2 (Fig 5B). This modest
374 decrease of H3K9me2 might be explained by the hypomorphic nature of the mutation or by a
375 functional redundancy between MAT isoforms that share over 85% amino acid sequence identity (SI
376 Appendix, Fig S11B). To test this hypothesis, we took advantage of a homozygous, mono-insertional,
377 co-suppressor transgenic line obtained during the process of generating *MAT3-YFP* overexpressors,
378 that we referred to as *MAT* KD (Fig 5C, SI Appendix, Fig S11C). Owing to their high DNA sequence
379 identity (SI Appendix, Fig S11D), all *MAT* genes are downregulated in this line (SI Appendix, Fig S11E).
380 In addition, the stochastic silencing of *MATs* gives rise to different phenotype severities: mildly
381 affected *MAT* KD plants (Fig 5C) that accumulate less *MATs* transcripts than wt (SI Appendix, Fig
382 S11E) and present a more severe phenotype than *mat3* hypomorphic mutant plants (Fig 5C); and
383 strongly affected *MAT* KD+ sister plants (Fig 5C) that accumulate even less *MAT* transcripts (SI
384 Appendix, Fig S11E). As anticipated, the H3K9me2 decrease was even more pronounced in *MAT* KD
385 plants than in *mat3* (Fig 5B). These results suggest that MAT isoforms possibly have additive roles in
386 H3K9 dimethylation. Given the decrease of H3K9me2 in MAT-deficient plants, we then determined

the extent of TE reactivation in *mat3* and *MAT* KD by RT-qPCR analysis of the same four TEs. We observed increased levels of TE transcripts in *mat3* (Fig 5D). This increase was generally more pronounced in *MAT* KD plants, particularly in *MAT* KD+ plants (Fig 5D). In contrast, we did not observe any significant effect on EI gene expression (SI Appendix, Fig S11F).

Topo VI favors MAT enrichment at some heterochromatin borders and depletion from euchromatic islands

Collectively, our results suggest that Topo VI and MAT3 could act together in maintaining sharp chromatin boundaries by influencing H3K9me2 deposition. We therefore used a newly developed anti-MAT antibody (Agrisera, Vännäs, Sweden) to test for MAT enrichment at specific loci and a putative Topo VI dependency. First, the specificity of this antibody was validated by immunoblot analysis of protein extracts from wt, *MAT* KD and *MAT3-YFP* overexpressing lines (SI Appendix, Fig S12A). We then performed ChIP-qPCR using an anti-MAT antibody and chromatin from wt and *caa39* plants, to measure the recovery of TEs that are reactivated upon Topo VI or MATs loss of functions. Interestingly, MATs were enriched on all the tested TEs in wt and less in *caa39*, as compared to an IgG negative control (Fig 6A). To specifically evaluate the implication of the BIN4/MID-associated MAT3 isoform, we performed ChIP-qPCR using an anti-GFP antibody and chromatin from two independent MAT3-YFP expressing lines. TEs reactivated in *MAT* KD and in Topo VI mutant plants were also specifically enriched in the GFP-pulled down chromatin (SI Appendix, Fig S12B). These results indicate that Topo VI is required for the association of MAT3 with heterochromatic elements.

To test whether Topo VI might also influence the enrichment of MATs at EIs, we performed ChIP-qPCR using an anti-MAT antibody and chromatin from wt and *caa39*, and analyzed the same EI as in Figures 4E and I, which shows increased H3K9me2 levels within the island body (probe 3-4) but decreased levels in the 5' heterochromatic border (probe 1) in *caa39* (Fig 4E and I, Fig 6B, top panel). We detected a significant decrease of MAT occupancy in this border in *caa39* (Fig 6B, bottom panel, probe 1) and, conversely, significantly enhanced MAT occupancy in the island body (probe 3) in *caa39* compared to wt (Fig 6B, bottom panel, probes 3-4). We analyzed three other S-EIs that show decreased gene expression levels (Fig 3C), increased internal H3K9me2 levels (Figs 4C and SI Appendix, Fig S8) and contain a single gene (*At4g06634*'s and *At5g30495*'s EIs) or two genes (*At2g07340*'s EIs). We observed trends of decreased MAT occupancy at one or both borders and enhanced MAT occupancy in the island bodies of *caa39* (Fig 6C-E). These results suggest that the loss

419 of Topo VI leads to MAT redistribution over Els, which correlates with H3K9me2 redistribution and
420 Els heterochromatinization in *caa39*.

Discussion

The *Arabidopsis* epigenome is largely indexed by discrete chromatin signatures usually corresponding to single genetic element (e.g., a gene or a TE) (49, 54). However, despite this, in *Arabidopsis* DNA methylation has a known tendency to spread away from many TEs (55), and a few other studies have reported the existence of heterochromatin spreading in plants (56–58). Yet, the mechanisms that repress heterochromatin spreading, hence safeguarding EIs, are poorly understood in plants. Our study confirmed the existence of an insulator-like mechanism that preserves EIs and unveiled the role played by the Topo VI complex in this process. We first provide evidence that Topo VI is required to preserve the euchromatic nature and transcriptional activity of gene islands within pericentromeric and chromosome 4 knob heterochromatic regions. Indeed, the most remarkable effect of the *caa39* mutation was the specific misregulation of pericentromeric elements, with a general downregulation of EI genes and, inversely, a reactivation of some heterochromatic TEs. We confirmed this peculiar expression pattern in several amorphic and hypomorphic mutants of the Topo VI complex. Surprisingly, EI gene downregulation is more pronounced in the hypomorphic mutants *caa39* and *BIN4* KD than in the corresponding null Topo VI mutants that display more severe growth defects. Taking advantage of uncoupled growth defects and gene expression changes in the hypomorphic *caa39* allele, we were able to show that the repression of EI genes is correlated with the invasion of EIs by H3K9me₂, indicating that Topo VI is required to prevent the spreading of H3K9me₂, here referred to as a boundary function. The increased expression of some EI genes in the quadruple mutant *caa39 suvh456*, defective for the H3K9 methylase SUVH4, SUVH5 and SUVH6, as compared with *caa39*, further supported that H3K9me₂ spreading over EI genes participates to some extent in the transcriptional silencing of EI genes in Topo VI defective plants.

Although it is known that CHG methylation is maintained through a feedback loop with H3K9me₂, WGBS identified no global increase of cytosine methylation over EIs in *caa39*, but rather a slight decrease of CHG methylation, suggesting that DNA methylation is not involved in the reduced expression of EI genes in Topo VI mutants. Other recent work has also shown that, under specific circumstances, increased H3K9me₂ levels do not necessarily result in increased CHG or CHH methylation, and vice versa. For instance, the AT-hook protein AHL10 ectopically recruits H3K9me₂ to small, AT-rich TEs without coincidental increase in DNA methylation (59). Conversely, the expression of *AtCMT3* in *Eutrema Salsugineum*, a Brassicaceae that has lost *CMT3* and gene body methylation, induces *de novo* gene body methylation in CHG, CHH and CG contexts, but without resulting in stable gain of H3K9me₂. Interestingly, CHG hypermethylation in gene bodies is also not correlated with consistent changes in gene expression in this case (60). While DNA methylation does not appear to be involved in the reduced expression of EI genes in Topo VI mutants, the question of

the relative importance of H3K9me2 remains. Indeed, and firstly, the level of H3K9me2 in EIs of *caa39* is still significantly lower than in canonical heterochromatin. This might result from histone H3 demethylation, a process that is likely still active in *caa39*. Alternatively, gain of H3K9me2 could be the outcome of a subset of cells in which *caa39* mutation has a strong effect on H3K9me2 boundaries. Secondly, the negative correlation between EI gene expressions and H3K9me2 changes is good, particularly in small EIs, but not very high, suggesting that H3K9me2 spreading over EI genes cannot entirely explain the transcriptional silencing of EI genes. H3K9me2 spreading on EIs might, in turn, affect the establishment of other chromatin modifications. For instance, in the *ibm1* mutant, increased levels of H3K9me2 on gene bodies are associated with decreased levels of H3K4me1 and transcriptional silencing (61). Conversely, in the *svh456* triple mutant, many TEs show a drastic increase in H3K4me1 level, which is associated with transcriptional derepression and loss of H3K9me2 (61). Therefore, it is plausible that other histone methylation changes also occur in *caa39*, as we did observe for H3K27me3, which shows an opposite trend to H3K9me2 in EIs. Thus, H3K9me2 spreading might itself perturb H3K27me3 deposition by PRC2 and/or erasing by trithorax group (trxG) proteins. This second hypothesis is supported by similar observations made in other organisms, where the loss of Swi6/HP1 leads to H3K9me2 spreading across natural constitutive heterochromatin boundaries in fission yeast (62), and alters H3K27me3 deposition on facultative heterochromatin in *Neurospora crassa* (63).

In animals, insulator proteins like CTCF can participate in several distinct processes, e.g. locally as a chromatin barrier and more globally on the formation of topologically associating domains (64). Similarly, the disorganization of chromocenters and the partial loss of pericentromeric TE silencing observed in Topo VI mutants might result from the loss of a local boundary function and, possibly, also by the loss of a distinct, more global, architectural function of Topo VI in heterochromatin condensation. Indeed, given that no obvious loss of DNA methylation and only a partial decrease of H3K9me2 over TEs were observed in Topo VI mutant plants, the reactivation of TEs is unlikely to be solely explained by decreased levels of these marks, but rather by a combined loosening of their heterochromatic nature and of their higher order organization. Although causal link between chromatin reorganization and TEs reactivation in plants is very disputed, a few recent studies link chromatin organizers with TE derepression independently of DNA demethylation. For instance, the natural depletion of histone 1 in sex cells is responsible of the reactivation of approx. 100 heterochromatic TEs via DNA demethylation-dependent (77/98) and -independent (21/98) mechanisms (65). In addition, MORC proteins, which belong to the GHKL ATPases superfamily like Topo VI, are required for the silencing of approx. 20 TEs and the formation of chromocenters without impacting H3K9me2 and DNA methylation levels (66–68). Interestingly human CTCF has been shown

to interact with Topo II β (69, 70) and appears to be part of a protein interaction network that also contains MORC2 and members of the cohesin complex in Hela cells (71). Intriguingly, plant and human recombinant MORC proteins seem to display a type II topoisomerase-like activity, which requires additional plant extracts for full activity (72).

Given the function of MAT enzymes in the synthesis of SAM, MAT perturbation is expected to affect a wide range of methylation reactions, which include DNA and histone methylations. The *mat3* mutant line used in our study has been shown, however, to have global SAM levels similar to wt and only very slightly reduced global levels of DNA methylations, unlike other *mat* mutants that show more severe DNA and histone methylation defects (73). This suggests that the increased levels of some TE transcripts in *mat3*, and the corresponding decreased levels of H3K9me2, are more likely attributable to a local effect of the *mat3* mutation, rather than a global decrease of SAM, or be the outcome of a subset of cells in which *mat3* mutation has a strong effect. Our finding that the Topo VI BIN4 subunit directly interacts with MAT3 and is required for MAT3 enrichment at some TE loci and depletion from euchromatic islands, might provide a mechanistic explanation for such a local role of MAT3 on chromatin, in addition to its general role in SAM synthesis (73). Similarly, the mammal MATII α isoform also directly supplies SAM in the close vicinity of oncogenes to allow transcriptional repression and H3K9me2 deposition (74, 75). Intriguingly, the mouse MATII α has been found to interact with Topoisomerase II α , a type IIA topoisomerase whose C-terminal regulatory domain possesses sequence similarity with the BIN4 subunit of the plant Topo VI complex (38). Hence, although this requires testing in other organisms, an interaction between MAT enzymes and type II topoisomerases might be evolutionary conserved. Targeting of MATs to specific chromatin regions by topoisomerases might be a way to couple SAM synthesis and availability *in situ*, possibly for DNA or histone methylation. Extensive genome-wide studies will provide a general view of chromatin modification changes in different *mat* mutants and their relative impacts on TE and gene expression.

In plants, the existence of an insulator-like function that would partition chromatin into different functional domains has long been questioned (9, 11, 26). We show that Topo VI participates to such a function by preventing the spreading of the heterochromatic mark H3K9me2 into neighboring euchromatin islands. Our results suggest that the prevention of heterochromatin spreading might rely upon a Topo VI-MAT3 interaction that would be important for the proper targeting of MAT3 to heterochromatin and its exclusion from euchromatic islands. Future studies might allow the identification of direct molecular links between Topo VI, MAT proteins and methyltransferases involved in DNA and histone methylation, for fine-tuning the establishment of sharp transitions in chromatin identity along the genome.

Materials and Methods

Detailed descriptions of the experimental methods are provided in SI Appendix, Supplementary Materials and Methods. These include cloning procedures, plant material and growth conditions, DNA preparation, Chop- and ChIP-qPCR, anti-5-meC ELISA assay, yeast two-hybrid screen, co-immunoprecipitation-MS, Western blot, RNA extraction, RT-qPCR and microarrays, RNA-seq library preparation and sequencing, RNA-seq bioinformatic treatment and analysis, whole-genome bisulfite sequencing and DNA methylation analysis, chromatin immunoprecipitation, ChIP-seq analysis, immunofluorescence, transient transformation and protoplasts preparation, confocal and epifluorescence microscopy.

Availability of data and material

ChIP-seq, RNA-seq, BS-seq and microarray datasets are available at <https://www.ncbi.nlm.nih.gov/geo/query/acc.cgi?acc=GSE103924> (reviewer token: slchuqakvwwfpsi). Custom scripts used in this study are available at <https://github.com/michel-teresse>.

Acknowledgments

We thank Imen Mestiri (IBENS, Paris) for her expertise with cytogenetics. We also want to express our gratitude to students who contributed to this work, especially Justine Quillet, Julien Vieu and César Botella. We thank Ben Field for critical reading of the manuscript. This work was supported by the French National Research Agency (ANR 2010-JCJC-1205-01 and ANR-14-CE02-0010 to CL). Work by FB was supported by the Investissements d'Avenir LabexMemory in Living Systems (MEMOLIFE) grant ANR-10-LABX-54. LD was supported by CEA and Région PACA. High-throughput RNA-sequencing was performed at the POPS platform, supported by the LabEx Saclay Plant Sciences-SPS (ANR-10-LABX-0040-SPS). MS analysis was performed at the IMM platform supported by a grant from GIS IBiSA. High-throughput ChIP-seq was performed at the TGML platform, supported by grants from Inserm, GIS IBiSA, Aix-Marseille Université, and ANR-10-INBS-0009-10.

Author contributions

LVM, FV, CV, LD, MR, and CB performed the experiments. CL and MT performed the bioinformatic analyses. LST was in charge of the sequencing. LVM, CL, FB and CL analyzed the data. LVM, KS, FB and CL designed the research. LVM, FB and CL wrote the manuscript. All authors read and approved the final manuscript.

Conflict of interest

The authors declare that they have no conflict of interest

References

1. J. Wang, S. T. Lawry, A. L. Cohen, S. Jia, Chromosome boundary elements and regulation of heterochromatin spreading. *Cell. Mol. Life Sci.* **71**, 4841–4852 (2014).
2. H. J. Muller, Types of visible variations induced by X-rays in *Drosophila*. *J. Genet.* **22**, 299–334 (1930).
3. T. Ali, R. Renkawitz, M. Bartkuhn, Insulators and domains of gene expression. *Curr. Opin. Genet. Dev.* **37**, 17–26 (2016).
4. W. A. Bickmore, B. van Steensel, Genome Architecture: Domain Organization of Interphase Chromosomes. *Cell* **152**, 1270–1284 (2013).
5. J. Dekker, T. Misteli, Long-Range Chromatin Interactions. *Cold Spring Harb. Perspect. Biol.* **7**, a019356 (2015).
6. J. R. Dixon, *et al.*, Topological domains in mammalian genomes identified by analysis of chromatin interactions. *Nature* **485**, 376–380 (2012).
7. B. Bonev, G. Cavalli, Organization and function of the 3D genome. *Nat. Rev. Genet.* **17**, 772–772 (2016).
8. P. Heger, B. Marin, M. Bartkuhn, E. Schierenberg, T. Wiehe, The chromatin insulator CTCF and the emergence of metazoan diversity. *Proc. Natl. Acad. Sci.* **109**, 17507–17512 (2012).
9. C. Wang, *et al.*, Genome-wide analysis of local chromatin packing in *Arabidopsis thaliana*. *Genome Res.* **25**, 246–256 (2015).

- 579 10. S. D. Singer, J. M. Hily, K. D. Cox, Analysis of the enhancer-blocking function of the TBS
580 element from *Petunia hybrida* in transgenic *Arabidopsis thaliana* and *Nicotiana tabacum*.
581 *Plant Cell Rep.* **30**, 2013–2025 (2011).
- 582 11. C. Liu, Y.-J. Cheng, J.-W. Wang, D. Weigel, Prominent topologically associated domains
583 differentiate global chromatin packing in rice from *Arabidopsis*. *Nat. Plants* **3**, 742–748 (2017).
- 584 12. C. Liu, D. Weigel, Chromatin in 3D: progress and prospects for plants. *Genome Biol.* **16**, 170
585 (2015).
- 586 13. J. Sequeira-Mendes, C. Gutierrez, Genome architecture: from linear organisation of chromatin
587 to the 3D assembly in the nucleus. *Chromosoma* **125**, 455–469 (2016).
- 588 14. S. Grob, M. W. Schmid, N. W. Luedtke, T. Wicker, U. Grossniklaus, Characterization of
589 chromosomal architecture in *Arabidopsis* by chromosome conformation capture. *Genome*
590 *Biol.* **14**, R129 (2013).
- 591 15. S. Grob, M. W. Schmid, U. Grossniklaus, Hi-C Analysis in *Arabidopsis* Identifies the KNOT , a
592 Structure with Similarities to the flamenco Locus of *Drosophila*. *Mol. Cell* **55**, 678–693 (2014).
- 593 16. S. Feng, *et al.*, Genome-wide Hi-C Analyses in Wild-Type and Mutants Reveal High-Resolution
594 Chromatin Interactions in *Arabidopsis*. *Mol. Cell* **55**, 694–707 (2014).
- 595 17. A. Veluchamy, *et al.*, LHP1 Regulates H3K27me3 Spreading and Shapes the Three-Dimensional
596 Conformation of the *Arabidopsis* Genome. *PLoS One* **11**, e0158936 (2016).
- 597 18. C. Liu, *et al.*, Genome-wide analysis of chromatin packing in *Arabidopsis thaliana* at single-
598 gene resolution. *Genome Res.* **26**, 1057–1068 (2016).
- 599 19. P. Fransz, H. De Jong, From nucleosome to chromosome: A dynamic organization of genetic
600 information. *Plant J.* **66**, 4–17 (2011).
- 601 20. L. Simon, M. Voisin, C. Tatout, A. V. Probst, Structure and function of centromeric and
602 pericentromeric heterochromatin in *Arabidopsis thaliana*. *Front. Plant Sci.* **6**, 1–8 (2015).
- 603 21. S. Del Prete, J. Arpón, K. Sakai, P. Andrey, V. Gaudin, Nuclear Architecture and Chromatin
604 Dynamics in Interphase Nuclei of *Arabidopsis thaliana*. *Cytogenet. Genome Res.* **143**, 28–50
605 (2014).
- 606 22. P. Fransz, J. H. de Jong, M. Lysak, M. R. Castiglione, I. Schubert, Interphase chromosomes in
607 *Arabidopsis* are organized as well defined chromocenters from which euchromatin loops
608 emanate. *Proc. Natl. Acad. Sci.* **99**, 14584–14589 (2002).

- 609 23. W. J. J. Soppe, *et al.*, DNA methylation controls histone H3 lysine 9 methylation and
610 heterochromatin assembly in Arabidopsis. *EMBO J.* **21**, 6549–6559 (2002).
- 611 24. O. Mathieu, A. V Probst, J. Paszkowski, Distinct regulation of histone H3 methylation at lysines
612 27 and 9 by CpG methylation in Arabidopsis. *EMBO J.* **24**, 2783–2791 (2005).
- 613 25. Z. Lippman, *et al.*, Role of transposable elements in heterochromatin and epigenetic control.
614 *Nature* **430**, 471–476 (2004).
- 615 26. Z. Vergara, C. Gutierrez, Emerging roles of chromatin in the maintenance of genome
616 organization and function in plants. *Genome Biol.* **18**, 96 (2017).
- 617 27. A. Bergerat, D. Gabelle, P. Forterre, Purification of a DNA topoisomerase II from the
618 hyperthermophilic archaeon *Sulfolobus shibatae*. A thermostable enzyme with both bacterial
619 and eucaryal features. *J. Biol. Chem.* **269**, 27663–27669 (1994).
- 620 28. A. Bergerat, *et al.*, An atypical topoisomerase II from archaea with implications for meiotic
621 recombination. *Nature* **386**, 414–417 (1997).
- 622 29. K. Schneider, *et al.*, The ROOT HAIRLESS 1 gene encodes a nuclear protein required for root
623 hair initiation in Arabidopsis. *Genes (Basel)*. **12**, 2013–2021 (1998).
- 624 30. K. Schneider, B. Wells, L. Dolan, K. Roberts, Structural and genetic analysis of epidermal cell
625 differentiation in Arabidopsis primary roots. *Development* **124**, 1789–1798 (1997).
- 626 31. K. Sugimoto-Shirasu, *et al.*, RHL1 is an essential component of the plant DNA topoisomerase
627 VI complex and is required for ploidy-dependent cell growth. *Proc. Natl. Acad. Sci. U. S. A.*
628 **102**, 18736–41 (2005).
- 629 32. H. J. Yoon, *et al.*, Lotus japonicus SUNERGOS1 encodes a predicted subunit A of a DNA
630 topoisomerase VI that is required for nodule differentiation and accommodation of rhizobial
631 infection. *Plant J.* **78**, 811–821 (2014).
- 632 33. F. Hartung, H. Puchta, Molecular characterization of homologues of both subunits A (SPO11)
633 and B of the archaebacterial topoisomerase 6 in plants. *Gene* **271**, 81–86 (2001).
- 634 34. F. Hartung, *et al.*, An archaebacterial topoisomerase homolog not present in other eukaryotes
635 is indispensable for cell proliferation of plants. *Curr. Biol.* **12**, 1787–1791 (2002).
- 636 35. Y. Yin, *et al.*, A crucial role for the putative Arabidopsis topoisomerase VI in plant growth and
637 development. *Proc. Natl. Acad. Sci. U. S. A.* **99**, 10191–6 (2002).

- 638 36. A. Mittal, *et al.*, TOPOISOMERASE 6B is involved in chromatin remodelling associated with
639 control of carbon partitioning into secondary metabolites and cell walls, and epidermal
640 morphogenesis in Arabidopsis. *J. Exp. Bot.* **65**, 4217–4239 (2014).
- 641 37. K. Sugimoto-shirasu, N. J. Stacey, J. Corsar, K. Roberts, M. C. Mccann, DNA Topoisomerase VI
642 Is Essential for Endoreduplication in Arabidopsis. *Curr. Biol.* **12**, 1782–1786 (2002).
- 643 38. C. Breuer, *et al.*, BIN4, a Novel Component of the Plant DNA Topoisomerase VI Complex, Is
644 Required for Endoreduplication in Arabidopsis. *Plant Cell* **19**, 3655–3668 (2007).
- 645 39. V. Kirik, A. Schrader, J. F. Uhrig, M. Hulskamp, MIDGET unravels functions of the Arabidopsis
646 topoisomerase VI complex in DNA endoreduplication, chromatin condensation, and
647 transcriptional silencing. *Plant Cell* **19**, 3100–3110 (2007).
- 648 40. E. L. Meczes, K. L. Gilroy, K. L. West, C. a Austin, The Impact of the Human DNA
649 Topoisomerase II C-Terminal Domain on Activity. *PLoS One* **3**, e1754 (2008).
- 650 41. A. Onoda, *et al.*, Nuclear dynamics of topoisomerase II β reflects its catalytic activity that is
651 regulated by binding of RNA to the C-terminal domain. *Nucleic Acids Res.* **42**, 9005–9020
652 (2014).
- 653 42. K. L. Gilroy, C. A. Austin, The Impact of the C-Terminal Domain on the Interaction of Human
654 DNA Topoisomerase II α and β with DNA. *PLoS One* **6**, e14693 (2011).
- 655 43. Y. Pommier, Y. Sun, S.-Y. N. Huang, J. L. Nitiss, Roles of eukaryotic topoisomerases in
656 transcription, replication and genomic stability. *Nat. Rev. Mol. Cell Biol.* **17**, 703–721 (2016).
- 657 44. M. Jain, A. K. Tyagi, J. P. Khurana, Overexpression of putative topoisomerase 6 genes from rice
658 confers stress tolerance in transgenic Arabidopsis plants. *FEBS J.* **273**, 5245–5260 (2006).
- 659 45. M. Jain, A. K. Tyagi, J. P. Khurana, Constitutive expression of a meiotic recombination protein
660 gene homolog, OsTOP6A1, from rice confers abiotic stress tolerance in transgenic Arabidopsis
661 plants. *Plant Cell Rep.* **27**, 767–778 (2008).
- 662 46. K. Simkova, *et al.*, Integration of stress-related and reactive oxygen species-mediated signals
663 by Topoisomerase VI in Arabidopsis thaliana. *Proc. Natl. Acad. Sci.* **109**, 16360–16365 (2012).
- 664 47. C. J. Underwood, I. R. Henderson, R. A. Martienssen, Genetic and epigenetic variation of
665 transposable elements in Arabidopsis. *Curr. Opin. Plant Biol.* **36**, 135–141 (2017).
- 666 48. K. De Preter, R. Barriot, F. Speleman, J. Vandesompele, Y. Moreau, Positional gene enrichment
667 analysis of gene sets for high-resolution identification of overrepresented chromosomal

668 regions. *Nucleic Acids Res.* **36**, 1–6 (2008).

669 49. J. Sequeira-Mendes, *et al.*, The Functional Topography of the Arabidopsis Genome Is
670 Organized in a Reduced Number of Linear Motifs of Chromatin States. *Plant Cell* **26**, 2351–
671 2366 (2014).

672 50. L. Shen, *et al.*, diffReps: Detecting Differential Chromatin Modification Sites from ChIP-seq
673 Data with Biological Replicates. *PLoS One* **8**, e65598 (2013).

674 51. H. Stroud, *et al.*, Non-CG methylation patterns shape the epigenetic landscape in Arabidopsis.
675 *Nat. Struct. Mol. Biol.* **21**, 64–72 (2014).

676 52. P. Zhang, MetaCyc and AraCyc. Metabolic Pathway Databases for Plant Research. *Plant*
677 *Physiol.* **138**, 27–37 (2005).

678 53. Y. Chen, T. Zou, S. McCormick, S -Adenosylmethionine Synthetase 3 Is Important for Pollen
679 Tube Growth. *Plant Physiol.* **172**, 244–253 (2016).

680 54. F. Roudier, *et al.*, Integrative epigenomic mapping defines four main chromatin states in
681 Arabidopsis. *EMBO J.* **30**, 1928–1938 (2011).

682 55. I. Ahmed, A. Sarazin, C. Bowler, V. Colot, H. Quesneville, Genome-wide evidence for local DNA
683 methylation spreading from small RNA-targeted sequences in Arabidopsis. *Nucleic Acids Res.*
684 **39**, 6919–6931 (2011).

685 56. S. R. Eichten, *et al.*, Spreading of Heterochromatin Is Limited to Specific Families of Maize
686 Retrotransposons. *PLoS Genet.* **8**, e1003127 (2012).

687 57. Z. Lang, *et al.*, The Methyl-CpG-Binding Protein MBD7 Facilitates Active DNA Demethylation to
688 Limit DNA Hyper-Methylation and Transcriptional Gene Silencing. *Mol. Cell* **57**, 971–983
689 (2015).

690 58. H. Saze, A. Shiraishi, A. Miura, T. Kakutani, Control of Genic DNA Methylation by a jmjC
691 Domain-Containing Protein in Arabidopsis thaliana. *Science (80-.)*. **319**, 462–465 (2008).

692 59. H. Jiang, *et al.*, Ectopic application of the repressive histone modification H3K9me2
693 establishes post-zygotic reproductive isolation in Arabidopsis thaliana. *Genes Dev.* **31**, 1272–
694 1287 (2017).

695 60. J. M. Wendte, *et al.*, Epimutations are associated with CHROMOMETHYLASE 3-induced de
696 novo DNA methylation. *Elife* **8** (2019).

- 697 61. S. Inagaki, *et al.*, Gene-body chromatin modification dynamics mediate epigenome
698 differentiation in *Arabidopsis*. *EMBO J.* **36**, 970–980 (2017).
- 699 62. R. Stunnenberg, *et al.*, H3K9 methylation extends across natural boundaries of
700 heterochromatin in the absence of an HP1 protein. *EMBO J.* **34**, 2789–2803 (2015).
- 701 63. K. Jamieson, *et al.*, Loss of HP1 causes depletion of H3K27me3 from facultative
702 heterochromatin and gain of H3K27me2 at constitutive heterochromatin. *Genome Res.* **26**,
703 97–107 (2016).
- 704 64. Y. Lu, G. Shan, J. Xue, C. Chen, C. Zhang, Defining the multivalent functions of CTCF from
705 chromatin state and three-dimensional chromatin interactions. *Nucleic Acids Res.* **44**, 6200–
706 6212 (2016).
- 707 65. S. He, M. Vickers, J. Zhang, X. Feng, Natural depletion of histone H1 in sex cells causes DNA
708 demethylation, heterochromatin decondensation and transposon activation. *Elife* **8**, 1–23
709 (2019).
- 710 66. G. Moissiard, *et al.*, MORC family ATPases required for heterochromatin condensation and
711 gene silencing. *Science* **336**, 1448–51 (2012).
- 712 67. Z. J. Lorkovi, U. Naumann, A. J. M. Matzke, M. Matzke, Involvement of a GHKL ATPase in RNA-
713 Directed DNA Methylation in *Arabidopsis thaliana*. *Curr. Biol.* **22**, 933–938 (2012).
- 714 68. T. R. Brabbs, *et al.*, The stochastic silencing phenotype of *Arabidopsis morc6* mutants reveals a
715 role in efficient RNA -directed DNA methylation. *Plant J.* **75**, 836–846 (2013).
- 716 69. M. Witcher, B. M. Emerson, Epigenetic Silencing of the p16INK4a Tumor Suppressor Is
717 Associated with Loss of CTCF Binding and a Chromatin Boundary. *Mol. Cell* **34**, 271–284
718 (2009).
- 719 70. T. M. Yusufzai, H. Tagami, Y. Nakatani, G. Felsenfeld, CTCF Tethers an Insulator to Subnuclear
720 Sites, Suggesting Shared Insulator Mechanisms across Species. *Mol. Cell* **13**, 291–298 (2004).
- 721 71. L. Uusküla-reimand, *et al.*, Topoisomerase II beta interacts with cohesin and CTCF at
722 topological domain borders. *Genome Biol.* **17**, 1–22 (2016).
- 723 72. M. Manohar, *et al.*, Plant and human MORC proteins have DNA modifying activities similar to
724 type II topoisomerases, but require additional factor(s) for full activity. *Mol. Plant. Microbe.*
725 *Interact.* **30**, 87–100 (2017).
- 726 73. J. Meng, *et al.*, METHIONINE ADENOSYLTRANSFERASE4 Mediates DNA and Histone

727 Methylation. *Plant Physiol.* **177**, 652–670 (2018).

728 74. Y. Katoh, *et al.*, Methionine Adenosyltransferase II Serves as a Transcriptional Corepressor of
729 Maf Oncoprotein. *Mol. Cell* **41**, 554–566 (2011).

730 75. Y. Kera, *et al.*, Methionine Adenosyltransferase II-dependent Histone H3K9 Methylation at the
731 COX-2 Gene Locus. *J. Biol. Chem.* **288**, 13592–13601 (2013).

732 76. H. Thorvaldsdóttir, J. T. Robinson, J. P. Mesirov, Integrative Genomics Viewer (IGV): High-
733 performance genomics data visualization and exploration. *Brief. Bioinform.* **14**, 178–192
734 (2013).

735

Figure legends

Figure 1. Topoisomerase VI is required for heterochromatin organization. (A) Representative nucleus ($n > 30$) from 6-day-old wt and *caa39* cotyledon epidermal cells stained with DAPI and showing indirect immunolocalization of H3K9me2. Scale bar: 5 μ m. (B) Two independently prepared nuclear extracts of wt and *caa39* were immunoblotted against H3 or H3K9me2, as indicated. (C) Same as (A) for 5-meC localization. (D) Elisa assay to quantify total 5-meC in 6-day-old cotyledons of wt, *caa39* and *ddm1-8*. **: $P < 0.005$ (Student's *t*-test).

Figure 2. Topo VI is required for the silencing of transposable elements. (A) Bar chart showing the proportions of reactivated TE superfamilies in *caa39* compared to the general proportion of TEs in the genome. The relative percentage is shown for each superfamily and the absolute number of reactivated TEs is noted above each bar. **: $P < 0.005$; ****: $P < 0.0001$ (Chi-squared test). (B) RT-qPCR confirmation of the reactivation of selected TEs in *caa39*, *rh12-1* and *bin4-1*. Error bars: \pm SEM of three biological replicates. *: $P < 0.05$; **: $P < 0.005$; ***: $P < 0.0005$ (Student's *t*-test). (C) DNA from indicated genotypes were extracted and digested with McrBC. The mean ratio of digested over undigested DNA from three biological replicates is shown. Error bars: \pm SEM of three biological replicates. *: $P < 0.05$; **: $P < 0.005$; ***: $P < 0.0005$ (Student's *t*-test). (D) Average distribution of methylated cytosine in CG, CHG and CHH contexts over TEs and 2 kb flanking regions. Two independent replicates for each genotype were performed. (E) ChIP-qPCR of H3K9me2 at selected TEs. Error bars: \pm SEM of three biological replicates. *: $P < 0.05$; **: $P < 0.005$; ***: $P < 0.0005$ (Student's *t*-test). (F) Average distribution of H3-normalized H3K9me2 over TEs and 2 kb flanking regions. Two (H3) and three (H3K9me2) independent biological replicates for each genotype were performed.

Figure 3. Genes in euchromatic islands within heterochromatic pericentromeric and chromosome 4 knob regions are repressed in Topo VI mutants. (A) Positional Gene Enrichment (PGE) analysis of the top 500 most downregulated genes in *caa39*. The bed files corresponding to coordinates of the widest enriched regions ($FDR < 0.05$) were visualized with a genome browser. Black lines correspond to enriched regions, blue boxes correspond to pericentromeric regions as defined by Yelina et al. (2012), green box to the knob and red to centromeres. (B) Scatter plots and Pearson correlations of differentially expressed ($P < 0.05$) pericentromeric genes in *caa39* and *bin4-1* or *bin4-2*. (C) RT-qPCR of selected pericentromeric genes in *caa39*, *rh12-1*, *bin4-1* and *BIN4* KD at 6 days post-germination. Error bars: \pm SEM of three biological replicates. **: $P < 0.005$; ***: $P < 0.0005$; ****: $P < 0.0001$ (two-

way ANOVA, Dunnett's test). (D) The proportion of each chromatin state was computed for EIs and their 1.5 kb flanking regions. EI: Euchromatic Islands. (E) Gene content in EIs.

Figure 4. Topo VI prevents the invasion of euchromatic islands by H3K9me2. (A) ChIP-qPCR analysis of H3K9me2 at EI genes. Error bars: \pm SEM of two biological replicates. *: $P < 0.05$; ***: $P < 0.0005$; ****: $P < 0.0001$ (two-way ANOVA, Fisher's test). (B) Average distribution of H3-normalized H3K9me2 along short euchromatic gene islands and 4 kb flanking regions. Two (H3) and three (H3K9me2) independent biological replicates for each genotype were performed. P -value was computed for each aggregated point by using the Mann-Whitney test. (C) Same as (B) long EIs. (D) Bar chart showing the average percentage of down or up H3K9me2 peaks identified by diffReps analysis in the genome, EIs, EI genes (EIGs), EI gene body, 5' and 3' UTRs. Error bars: \pm SEM of three biological replicates. *: $P < 0.05$; ***: $P < 0.0005$; ****: $P < 0.0001$ (two-way ANOVA, Fisher's test). (E) ChIP-qPCR validation of a single-gene island for H3K9me2. Error bars: \pm SEM of three biological replicates. *: $P < 0.05$; ****: $P < 0.0001$ (two-way ANOVA, Fisher's test). (F) Average distribution of methylated cytosine in CG, CHG and CHH contexts over EIs. Two independent replicates for each genotype were performed. (G) K-means linear clustering of H3K9me2 and H3K27me3 tag densities across EIs and their 900 nt flanking borders as revealed by seqMINER in *caa39* and wt. (H) Heatmap correlation clustering of EI genes with significant changes in RNA-seq and H3K9me2/H3 ChIP-seq. (I) Integrative Genomics Viewer (76) screenshot of H3, H3K9me2, H3K27me3, RNA, CG, CHG and CHH methylation profiles in wt and *caa39* on a single gene-containing island. Each track is normalized against corresponding input samples (ChIP-seq) and by the sequencing depth. Numbers indicate the position of primers used in (E).

Figure 5. MAT3 interacts with Topo VI and is required for H3K9me2 deposition on heterochromatic loci.

(A) Protoplasts from transiently agrotransformed *N. benthamiana* leaves expressing different combination of BiFC vectors, as indicated. Nuclei were stained with Hoechst 33342. (B) Chromatin of 3 week-old wt or *MAT* KD (here a mixed pool of *MATs* silenced plants with strong or weak phenotype) rosette leaves, or 6 day-old wt or *mat3* cotyledon nuclei was immunoprecipitated with anti-H3K9me2 antibodies and the recovery of TEs known to be reactivated in *caa39* was assessed by qPCR. The result is shown as a percentage of recovery normalized against wt. Error bars: \pm SEM of two biological replicates. *: $P < 0.05$; **: $P < 0.005$; ***: $P < 0.0005$; ****: $P < 0.0001$ (two-way ANOVA, Dunnett's test). (C) Representative photographs of 4-week-old wt, *MATs* silenced plants with

stronger (*MAT* KD+) and weaker (*MAT* KD) developmental phenotypes, and the *mat3* mutant. (D) RT-qPCR analysis of TE transcript abundance in indicated genotypes. Error bars: \pm SEM of three biological replicates. *: $P < 0.05$; **: $P < 0.005$; ***: $P < 0.0005$ (Student's *t*-test).

Figure 6. Topo VI is required for MAT enrichment at heterochromatin borders and exclusion from euchromatic islands. (A) Chromatin of 6-day-old wt or *caa39* cotyledon nuclei was immunoprecipitated with anti-MATs antibodies and the recovery of TEs reactivated in *MATs* silenced plants and *caa39* was measured by qPCR. Error bars: \pm SEM of three biological replicates. (B-E) Top panels: Integrative Genomics Viewer screenshots of H3- and sequencing depth-normalized H3K9me2 profiles, and locations of primers used in bottom panels. Bottom panels: Same as (A) on EIs containing repressed genes in *caa39* such as *AT1G41830* (B), *AT4G06634* (C), *AT2G07340* (D) and *AT5G30495* (E). Error bars: \pm SEM of two biological replicates. *: $P < 0.05$; **: $P < 0.005$; ***: $P < 0.0005$ (Student's *t*-test).

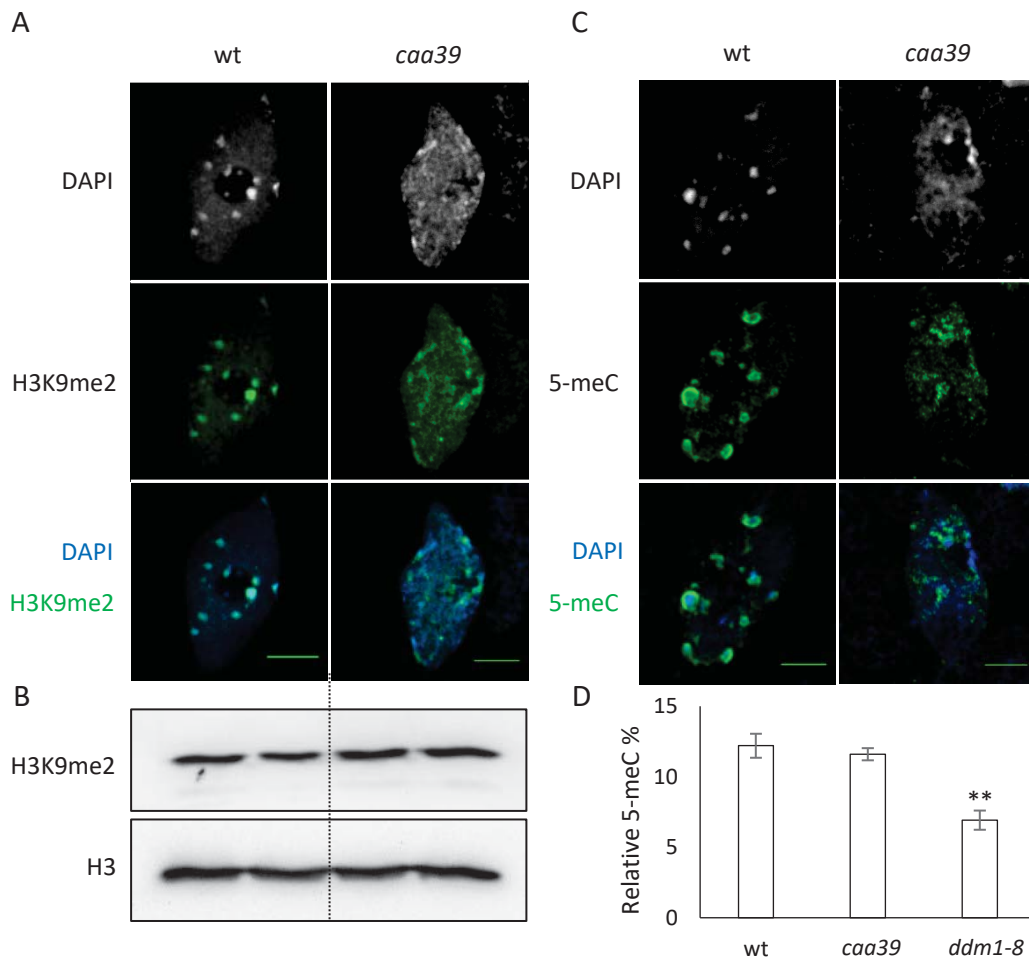


Fig 1

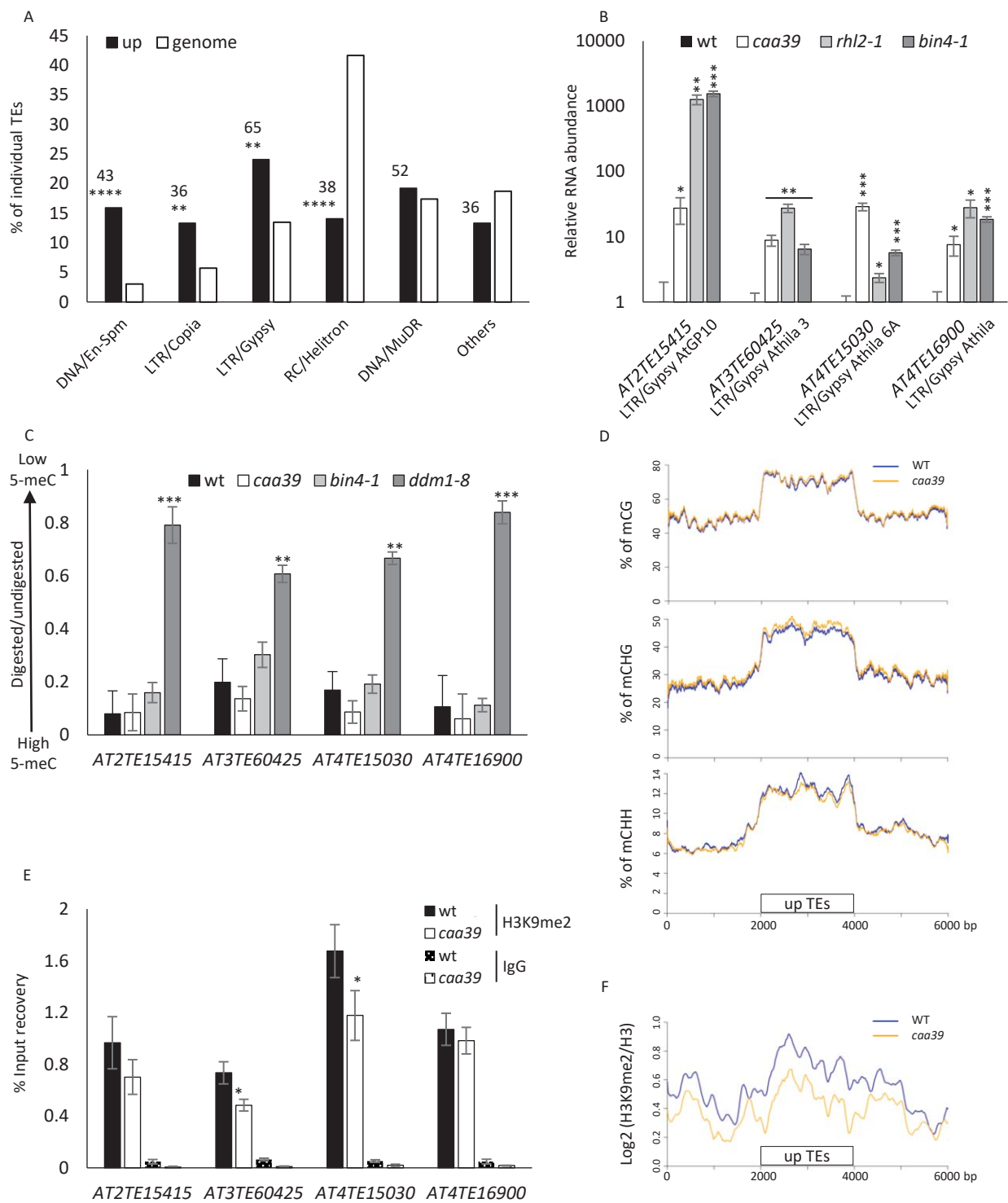


Fig 2

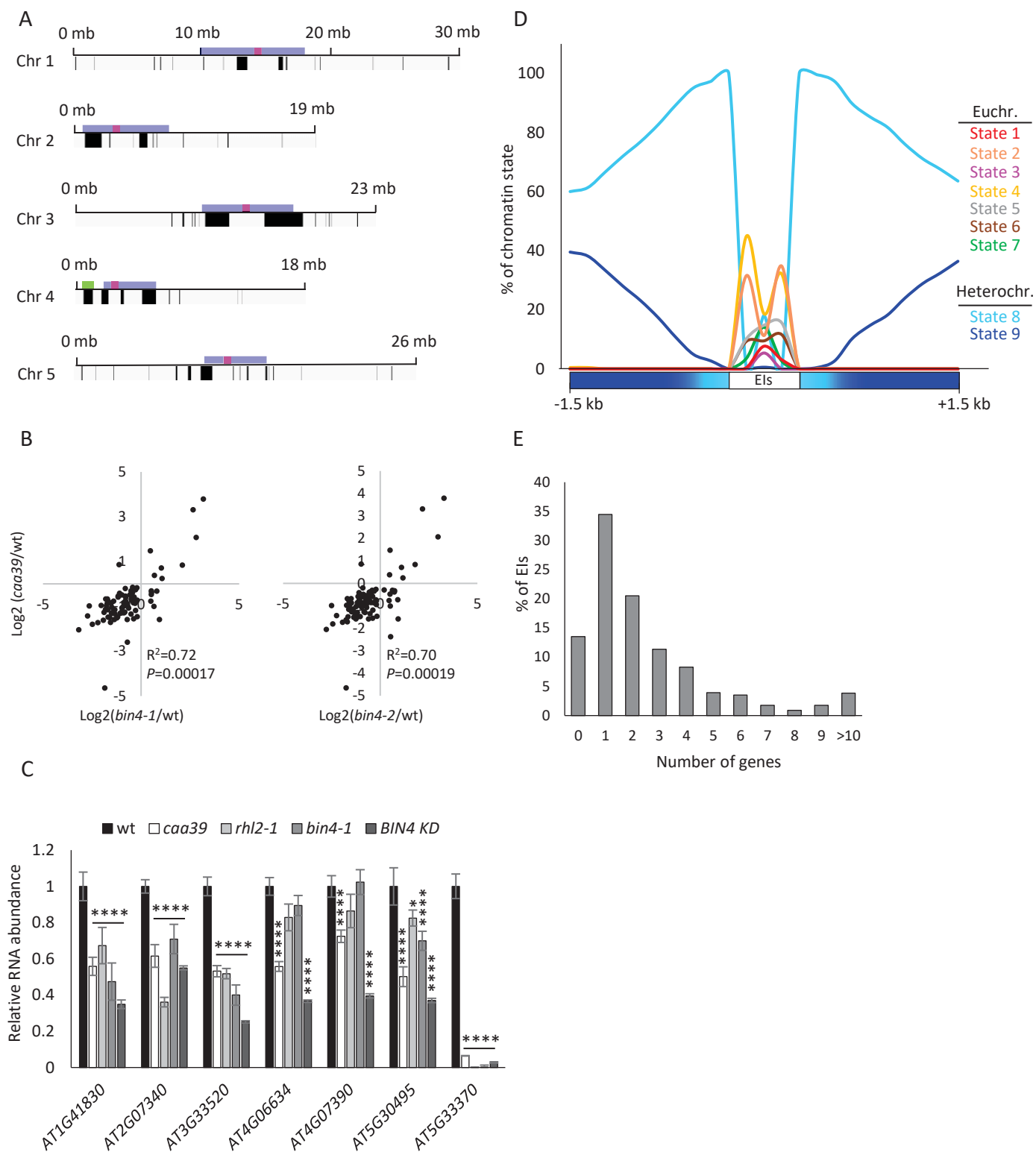


Fig 3

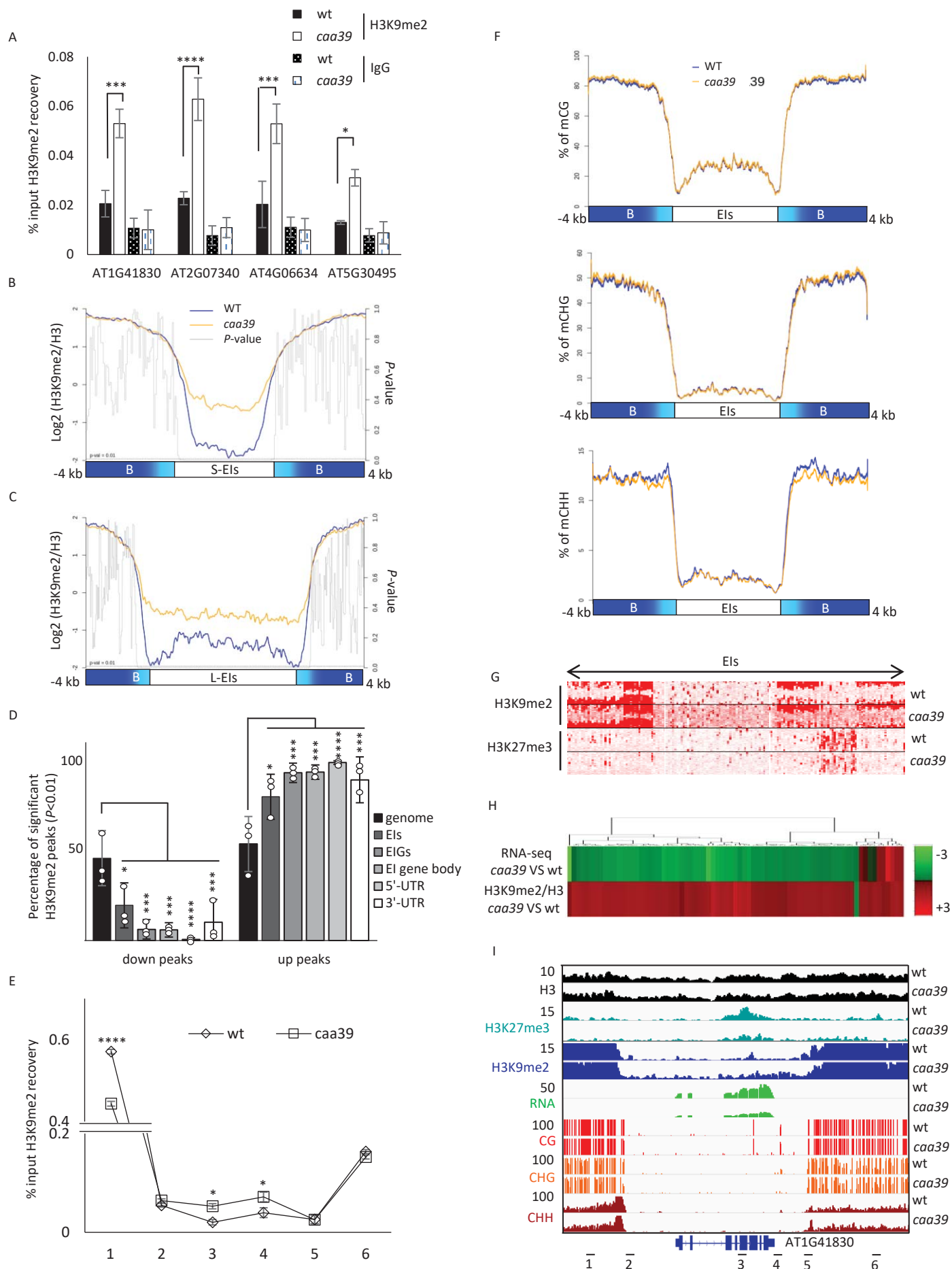


Fig 4

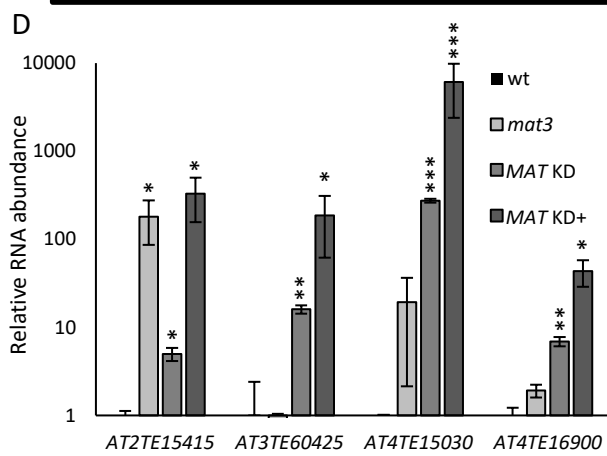
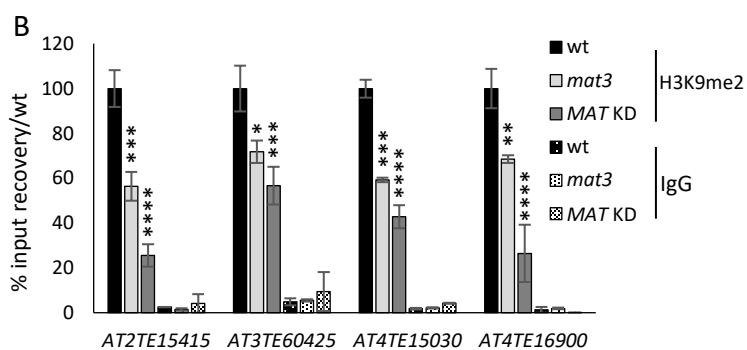
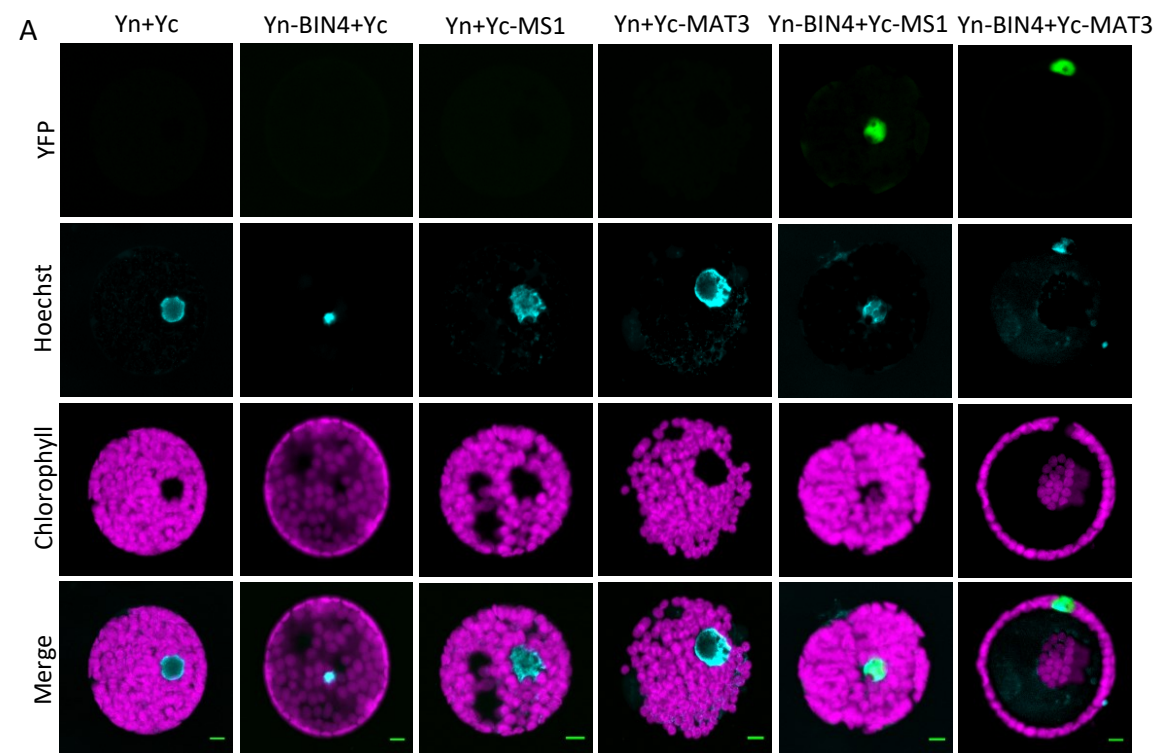


Fig 5

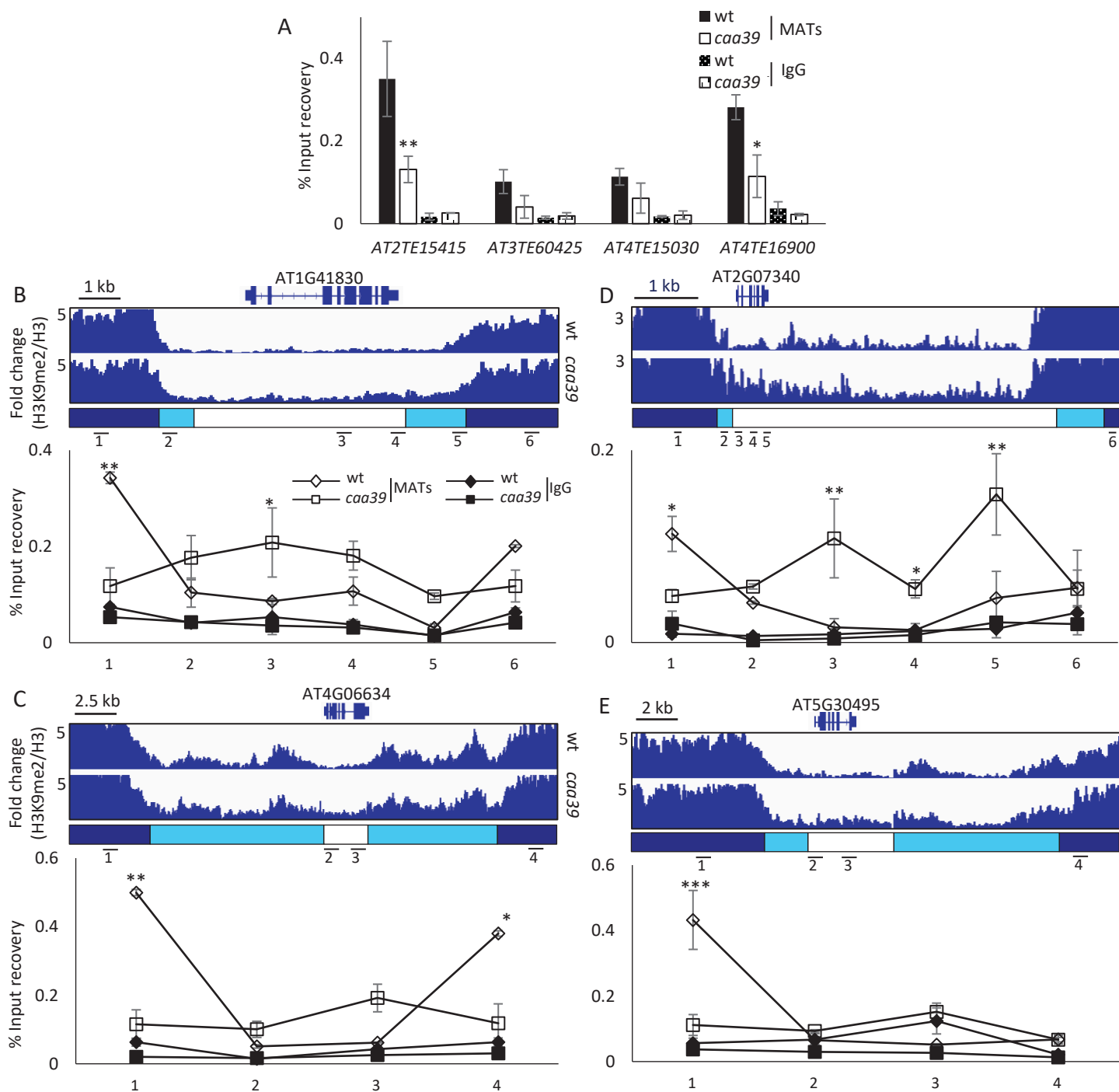


Fig 6